Am J Transl Res 2020;12(12):7885-7898
www.ajtr.org /ISSN:1943-8141/AJTR0125340

Original Article

CLOCK disruption aggravates carotid artery stenosis through endoplasmic reticulum stress-induced endothelial-mesenchymal transition

Hanfei Tang[1*], Song Xue[1*], Gefei Zhao[2*], Chao Fang[1], Liang Cai[1], Zhenyu Shi[1], Weiguo Fu[1], Ruizhe Qian[3], Pengfei Zhang[2], Xiao Tang[1], Daqiao Guo[1]

[1]Department of Vascular Surgery, Institute of Vascular Surgery, Zhongshan Hospital, Fudan University, Shanghai, China; [2]Department of Thoracic and Cardiovascular Surgery, The Affiliated Drum Tower Hospital, Medical School of Nanjing University, Nanjing, Jiangsu, China; [3]Department of Physiology and Pathophysiology, School of Basic Medical Sciences, Shanghai Key Laboratory of Clinical Geriatric Medicine, Fudan University, Shanghai, China. [*]Equal contributors.

Received October 31, 2020; Accepted November 18, 2020; Epub December 15, 2020; Published December 30, 2020

Abstract: Carotid artery stenosis is a leading cause of ischemic stroke, but the underlying mechanism remains unclear. We aimed to determine the molecular mechanisms of carotid plaque progression. We analyzed the molecular and morphometric characteristics of carotid plaque samples obtained from 30 patients who underwent carotid endarterectomy. Additionally, we established a mouse model of carotid atherosclerosis by partially ligating the left common carotid arteries of male *Clock*$^{\Delta 19/\Delta 19}$ (Clk) and wild-type (WT) C57BL/6J mice fed a high-fat diet. Clk and WT primary mouse aortic endothelial cells (pMAECs) were exposed to disturbed flow (DF) or undisturbed flow (UF) with or without treatment with the IRE-1α inhibitor STF-083010 or the PERK inhibitor GSK2606414. In human carotid artery plaques, *CLOCK* expression was lower in the lipid-rich necrotic core than in transitional regions, especially in the endothelium. Decreased *CLOCK* mRNA levels were associated with more extensive stenosis, intraplaque hemorrhage, and complex plaque in human carotid plaques. In mice, the *Clock*$^{\Delta 19/\Delta 19}$ mutation significantly increased neointima formation and neovascularization but decreased collagen content and lumen area in partially ligated carotid arteries. In addition, *Clock*$^{\Delta 19/\Delta 19}$ mutants exhibited significantly decreased Cdh5 expression and increased expression of endothelial-mesenchymal transition (EndMT) and endoplasmic reticulum (ER) stress markers in mice with partially ligated carotid arteries and pMAECs exposed to DF. Notably, inhibition of the IRE1α-XBP1 axis abrogated the increased EndMT caused by *Clock*$^{\Delta 19/\Delta 19}$ mutation and DF in pMAECs. In conclusion, the disruption of CLOCK function aggravates EndMT via the IRE1α-XBP1 axis, contributing to carotid artery stenosis.

Keywords: Carotid artery stenosis, circadian locomotor output cycles kaput, endothelial-mesenchymal transition, endoplasmic reticulum stress, disturbed flow

Introduction

Carotid artery stenosis contributes to the occurrence of ischemic stroke [1]. Therefore, determining the molecular mechanisms of carotid artery stenosis may help in preventing stroke. Carotid artery stenosis is a multistep cardiovascular disease promoted by aging, disturbed blood flow, hypercholesterolemia, hyperglycemia, and smoking [2]. Emerging evidence suggests that endothelial-mesenchymal transition (EndMT) in endothelial dysfunction is a crucial component and an emerging concept in the pathogenesis of vascular diseases [2]. Endothelial dysfunction is closely related to the excessive unfolded protein response (UPR) activated by endoplasmic reticulum (ER) stress [3-5]. However, the upstream regulator of ER stress and the mechanism through which ER stress induces EndMT during carotid artery stenosis remains unclear and needs to be clarified [6].

Proteins involved in UPR and ER chaperones are under the control of biological rhythms [7]. The circadian clock consists of positive and negative feedback control loops of approximately 24 h, which are regulated by core clock genes such as *CLOCK* and *BMAL1* [8]. The disruption of both central and peripheral *CLOCK*

genes is closely associated with the aging process and aging-related diseases such as atherosclerosis [9]. Thus, we hypothesized that the disruption of CLOCK expression in the carotid artery (CA) may lead to excessive ER stress and subsequent carotid artery stenosis.

Here, we investigated CLOCK expression in the carotid plaque tissues of patients with internal carotid artery stenosis (ICAS) and analyzed the correlation of CLOCK expression levels with the pathological features of carotid plaques. We also identified CLOCK as a suppressor of carotid plaque progression and explored the underlying mechanisms by which this may occur. Our data demonstrate that inhibiting the IRE1α-XBP1 axis significantly attenuates the endothelial-to-mesenchymal transition (EndMT) induced by disturbed flow (DF) and the disturbance of CLOCK expression, thereby inhibiting carotid plaque progression.

Materials and methods

Human tissue samples and ethics statement

Experiments involving human samples were approved (IRB approval No. Y2019-219) and supervised by the Ethics Committee of Zhongshan Hospital (Shanghai, China). Clinical carotid plaque specimens were used in accordance with the Declaration of Helsinki, and written informed consent was obtained from all patients. Samples were consecutively obtained from 30 patients who underwent carotid endarterectomy for ICAS at 8:00-10:00 AM following Clinical Practice Guidelines between February 1, 2018, and January 31, 2019 [10]. Samples were stored at -80°C or formalin-fixed and paraffin-embedded until further use.

Animal studies with partial ligation

The *in vivo* studies were performed at Institute of Vascular Surgery, Zhongshan Hospital, Fudan University. All animal experiments were approved by the Institutional Animal Care and Use Committee of Zhongshan Hospital, Fudan University (Shanghai, China). Male *Clock*$^{\Delta 19/\Delta 19}$ (mutant) C57BL/6J mice, which showed reduced CLOCK mRNA levels and CLOCK function [11], and wild-type (WT) C57BL/6J mice were obtained from the Model Animal Research Center of Nanjing University (Jiangsu, China). All mice were fed a chow diet and water *ad libitum* until 6 weeks of age. Mice were then fed the Paigen high-fat diet (1.25% cholesterol, 15% fat, 0.5% cholic acid) and water *ad libitum* [12]. At 12 weeks, all mice were anesthetized in a closed chamber with 1-2% isoflurane in oxygen for 2 to 5 min until immobile and then underwent partial ligation of the left common CA and mock treatment of the right common CA at 8:00-10:00 AM [12]. All mice were sacrificed at week 18 by pentobarbital overdose. CA tissues were harvested, snap-frozen in liquid nitrogen, and stored at -80°C at 8:00-10:00 AM.

Endothelial cell (EC) isolation and culture

WT or *Clock*$^{\Delta 19/\Delta 19}$ primary mouse aortic ECs (pMAECs) were isolated and cultured as previously described [13]. Briefly, after adequate anesthesia, mouse aortas were separated and dissected into 2 mm sections that were then placed on Matrigel pre-coated plates. After culture in endothelial cell medium at 37°C for 7-14 days, pMAECs were passaged. At 8:00-10:00 AM, pMAECs at passage 5-6 were exposed to DF and undisturbed flow (UF) using a 10 mm-radius orbital shaking system at 210 rpm and dimethyl sulfoxide in the presence or absence of 15 or 30 μM STF-083010 (IRE-1α inhibitor; Selleckchem, Shanghai, China) or 0.015 or 0.03 μM GSK2606414 (PERK inhibitor; Selleckchem) for a further 72 h [14].

Western blotting

In pMAECs and the partially ligated CA, the relative protein expression levels of p-PERK, p-IRE1α, ATF6, p-eIF2α, XBP-1, and GAPDH were measured by western blotting using standard methods. Anti-ATF6 (ab37149) and anti-GAPDH (ab8245) antibodies were obtained from Abcam (Cambridge, MA, USA), anti-Xbp-1 (24385) was from Signalway Antibody (Baltimore, USA), anti-p-IRE1α (Ser724; ARG40603) and anti-p-eIF2α (Ser51; ARG57722) were from arigo Biolaboratories Corp (Taiwan), and anti-p-PERK (Thr980; 3179s) was from Cell Signaling Technology (Danvers, MA, USA). Band intensities were quantified using ImageJ software (https://imagej.nih.gov/ij/) and normalized to the levels of GAPDH.

Quantitative reverse transcription PCR (qRT-PCR)

TRIzol (Thermo Fisher Scientific, Waltham, MA, USA) was used to isolate total RNA from pMAECs. An Omniscript RT kit (Qiagen, Hilden,

Table 1. Primer sequences for the genes targeted in quantitative reverse transcription PCR

Target	GenBank accession no.	Primer sequence (5'-3')	Category
CLOCK	NM_004898	F: CAGGCAGCATTTACCAGCTCATG R: GTAGCTTGAGACATCACTGGCTG	Human Primer
GAPDH	NM_002046	F: GTCTCCTCTGACTTCAACAGCG R: ACCACCCTGTTGCTGTAGCCAA	Human Primer
S100a4	NM_011311	F: AGCTCAAGGAGCTACTGACCAG R: GCTGTCCAAGTTGCTCATCACC	Mouse Primer
Acta2	NM_007392	F: TGCTGACAGAGGCACCACTGAA R: CAGTTGTACGTCCAGAGGCATAG	Mouse Primer
Vimentin	NM_011701	F: CGGAAAGTGGAATCCTTGCAGG R: AGCAGTGAGGTCAGGCTTGGAA	Mouse Primer
Snai1	NM_011427	F: TGTCTGCACGACCTGTGGAAAG R: CTTCACATCCGAGTGGGTTTGG	Mouse Primer
Cdh5	NM_009868	F: GAACGAGGACAGCAACTTCACC R: GTTAGCGTGCTGGTTCCAGTCA	Mouse Primer
Mmp2	NM_008610	F: CAAGGATGGACTCCTGGCACAT R: TACTCGCCATCAGCGTTCCCAT	Mouse Primer
Mmp9	NM_013599	F: GCTGACTACGATAAGGACGGCA R: TAGTGGTGCAGGCAGAGTAGGA	Mouse Primer
Gapdh	NM_008084	F: CATCACTGCCACCCAGAAGACTG R: ATGCCAGTGAGCTTCCCGTTCAG	Mouse Primer

Germany) was used to synthesize first-strand complementary DNA. qRT-PCR using SYBR Green was used to quantify changes in mRNA levels. Expression levels were calculated using the $2^{-\Delta CT}$ method. All primers used are listed in **Table 1**.

Histological and morphometric analysis

Histological analysis of carotid arterial segments was performed as previously reported [12]. Briefly, samples were formalin-fixed and paraffin-embedded. The blocks were sectioned at 5 μm intervals using a microtome. The sections were then deparaffinized in xylene and rehydrated with graded ethanol before staining with hematoxylin-eosin or Masson's trichrome stain. The luminal, intimal, and medial areas of the vessel and percent area of collagen deposition were measured by two independent investigators blinded to the experimental design using ImageJ software.

Immunofluorescence and confocal microscopy

The carotid arterial segments were formalin-fixed and paraffin-embedded. The blocks were sectioned at 5 μm intervals using a microtome. The resulting sections were deparaffinized in xylene and dehydrated in an ethanol series (100%, 90%, 80%, 70%, and 50% ethanol), followed by rinsing with phosphate-buffered saline (PBS). Antigen retrieval was performed in citrate buffer (10 mM, pH 6.0) at 95°C. After cooling, the tissue slices were blocked for 1 h in 5% bovine serum albumin (BSA) and 20% donkey serum in PBS and then incubated with primary antibodies in 3% BSA overnight at 4°C in a humidified chamber. Primary antibodies used for mice immunofluorescence were anti-CD31 (550274; BD Biosciences), anti-S100A4 (ab-27957; Abcam), anti-vimentin (ab24525; Abcam), and anti-XBP-1 (sc-8015; Santa Cruz Biotechnology). Anti-CLOCK (ab3517; Abcam) antibody was used for human IF. After incubation with the primary antibodies, tissue sections were washed with Tris-buffered saline and incubated with cyanine-3 (Cy3) or fluorescein isothiocyanate-conjugated secondary antibodies for 1 h at 20°C. The sections were then observed and photographed using the Axiovert 200 M microscopy system (Carl Zeiss, Jena, Germany). The number of vimentin-, XBP-1-, or S100A4-positive ECs and neovessels (CD31-positive tubules) was quantified by two independent investigators blinded to the experimental design using ImageJ software.

Statistical analyses

Data are expressed as the mean ± standard deviation. All experiments were performed at least three times. Statistical comparisons between two groups were performed using

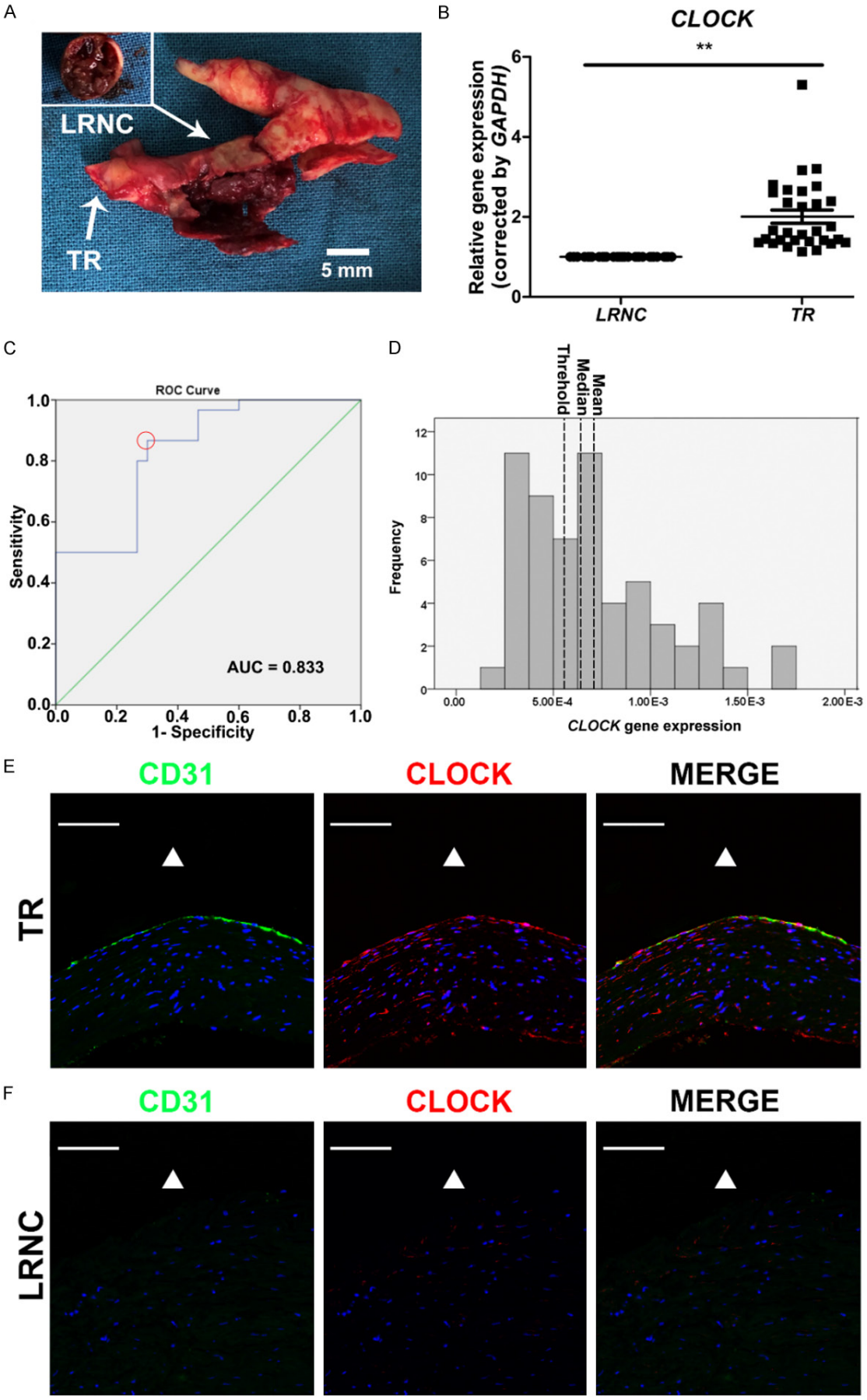
A
LRNC
TR
5 mm
B
CLOCK
**
Relative gene expression (corrected by GAPDH)
LRNC
TR
C
ROC Curve
Sensitivity
1- Specificity
AUC = 0.833
D
Threhold
Median
Mean
Frequency
CLOCK gene expression
E
CD31
CLOCK
MERGE
TR
F
CD31
CLOCK
MERGE
LRNC

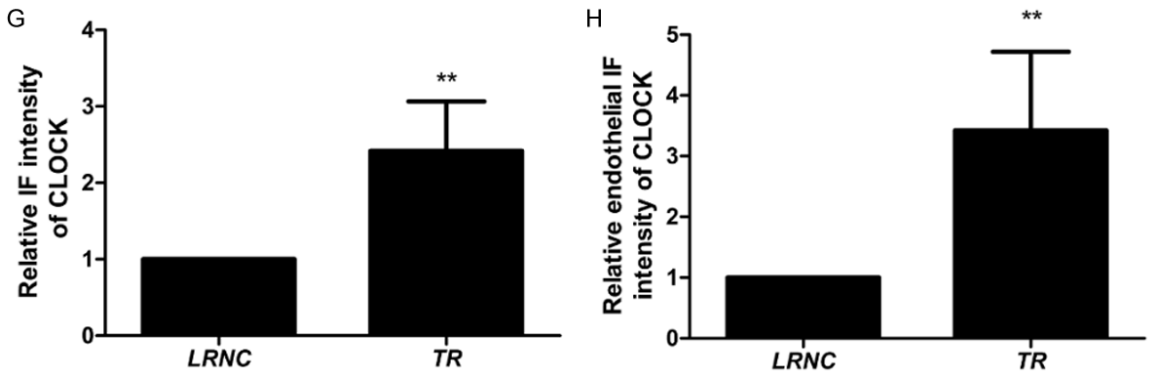

Figure 1. Decreased *CLOCK* mRNA levels were associated with the development of carotid atherosclerotic plaques. A. Morphology of the lipid-rich necrotic core (LRNC) with intraplaque hemorrhage and transitional region (TR) of carotid atherosclerotic plaque. B. *CLOCK* mRNA levels were detected in LRNC (n = 30) and TR (n = 30) of tissues from patients with internal carotid artery stenosis. C. Receiver-operating characteristic curve of *CLOCK* mRNA levels and TR (red dotted circle, optimal cut-off point). D. Histogram of *CLOCK* mRNA levels (left dotted line, threshold, 5.56×10^{-4}; middle dotted line, median, 6.38×10^{-4}; right dotted line, mean, 7.09×10^{-4}). AUC, area under curve. E, F. Immunofluorescence staining for CLOCK (red) and CD31 (green) of TR and LRNC. Nuclei were stained with 4',6-diamidino-2-phenylindole (DAPI; blue). The triangle indicates the lumen side. G. Immunofluorescence intensity of CLOCK in the TR and LRNC (n = 5). H. Endothelial immunofluorescence intensity of CLOCK in the TR and LRNC (n = 5). Scale bar: 100 μm. $^{**}P < 0.01$.

Student's *t*-test. For multiple comparison tests, one-way analysis of variance with Bonferroni's correction was employed. Comparisons of non-parametric data between two groups were performed using the two-tailed Mann-Whitney test. Differences were considered significant at $P < 0.05$. All these statistical analysis were performed using SPSS version 20.0 (SPSS Inc., Chicago, IL, USA).

Results

Expression of CLOCK in the lipid-rich necrotic core (LRNC) and transitional region (TR) tissues of carotid atherosclerotic plaques

LRNC and TR of carotid atherosclerotic plaque tissues were collected from 30 patients with ICAS (**Figure 1A**). *CLOCK* mRNA levels in LRNC tissues were much lower than those in the TR of the carotid atherosclerotic plaque tissues (**Figure 1B**). The potential cut-off values of the *CLOCK* mRNA level predicting LRNC formation were sequentially measured by receiver-operating characteristic curve analysis (**Figure 1C**). Using the maximum Youden index, the optimal cut-off value for dividing high and low levels of *CLOCK* mRNA was 5.56×10^{-4} (**Figure 1C**, **1D**). We thus defined a *CLOCK* mRNA level ≤ 5.56×10^{-4} as low *CLOCK* mRNA expression and a *CLOCK* mRNA level > 5.56×10^{-4} as high *CLOCK* mRNA expression (sensitivity = 86.70%, specificity = 70.00%). Low levels of *CLOCK* mRNA were found in 70% of LRNC specimens and 13.33% of TR tissue samples ($P < 0.001$; **Table 2**). Immunostaining demonstrated that CLOCK expression of the LRNC was significantly lower than that of the TR, especially in the endothelium (**Figure 1E-H**). Hence, *CLOCK* expression was low in the carotid atherosclerotic plaque tissues of patients with ICAS.

Correlation between CLOCK mRNA expression and clinicopathological plaque features

As shown in **Table 3**, LRNCs with low *CLOCK* mRNA levels were significantly and positively associated with the status of complex (AHA type VI) plaques, the extent of stenosis, and intraplaque hemorrhage (IPH).

$Clock^{\Delta 19/\Delta 19}$ mutation aggravated carotid artery stenosis in the partially ligated CA model

To confirm the suppressive effect of CLOCK on carotid artery stenosis, a partially ligated CA mouse model was employed. The luminal area of partially ligated CAs was smaller in $Clock^{\Delta 19/\Delta 19}$ mice than in WT mice, while the intimal area and intima/media ratio of partially ligated CAs was higher in $Clock^{\Delta 19/\Delta 19}$ mice than in WT mice (**Figure 2A-F**). Masson trichrome staining revealed that the relative collagen fractional area of partially ligated CAs were significantly lower

Table 2. *CLOCK* mRNA levels in the lipid-rich necrotic core and transitional region

Sample	n	Low *CLOCK* mRNA expression (% of samples)
Lipid-rich necrotic core	30	21 (70.00%)
Transitional region	30	4 (13.33%)*

*$P < 0.01$ in comparisons between tissue samples.

Table 3. Association of low *CLOCK* mRNA expression in the lipid-rich necrotic cores (LRNCs) with clinicopathological plaque features

Parameter	n	Low *CLOCK* mRNA expression (% of samples)	*P*
Sex			
Male	26	69.23%	0.822
Female	4	75.00%	
Age (years)			
55-75	16	81.25%	0.169
< 55	14	57.14%	
Hypertension			
Yes	15	73.33%	0.702
No	15	66.67%	
Diabetes mellitus			
Yes	18	77.78%	0.270
No	12	58.33%	
Hyperlipidemia			
Yes	17	76.47%	0.394
No	13	61.54%	
Smoking			
Yes	10	80.00%	0.416
No	20	65.00%	
Statin use			
Yes	26	69.23%	0.822
No	4	75.00%	
Extent of stenosis (NASCET)			
50-69%	7	28.57%	0.005
70-99%	23	82.61%	
Intraplaque hemorrhage			
Yes	15	93.33%	0.005
No	15	46.67%	
Surface defect			
Yes	7	85.71%	0.264
No	23	65.22%	
Complex (AHA type VI) plaque			
Yes	18	88.89%	0.012
No	12	41.67%	

Abbreviations: AHA, American Heart Association; NASCET, North American Symptomatic Carotid Endarterectomy.

in *Clock*$^{\Delta 19/\Delta 19}$ mice than in WT mice (**Figure 2A**, **2G**). In contrast, the relative collagen fractional area of CAs were comparable in the mock treatments of both mouse groups (**Figure 2A**, **2H**). Moreover, neovessel density of partially ligated CAs was higher in *Clock*$^{\Delta 19/\Delta 19}$ mice than in WT mice (**Figure 2B**, **2I**).

Clock$^{\Delta 19/\Delta 19}$ *mutation aggravated EndMT in the partially ligated CA*

We performed a set of experiments to investigate the effects of CLOCK on EndMT in the partially ligated CA. Double immunostaining demonstrated that the proportion of vimentin (+) or S100A4 (+) ECs was significantly higher in the intima of partially ligated CAs of *Clock*$^{\Delta 19/\Delta 19}$ mice than in those of WT mice (**Figure 3A-F**). Moreover, vimentin and S100A4 expression levels were significantly increased in the intima of partially ligated CAs of *Clock*$^{\Delta 19/\Delta 19}$ mice compared to WT mice (**Figure 3A-F**). qRT-PCR results demonstrated that the levels of the endothelial marker *Cdh5* were lower, while the levels of mesenchymal markers *S100a4, Acta2, vimentin, Twist1, Snai1, Mmp2*, and *Mmp9* were higher in the partially ligated CAs of *Clock*$^{\Delta 19/\Delta 19}$ mice than in the partially ligated CAs of WT mice (**Figure 3G**).

Clock$^{\Delta 19/\Delta 19}$ *mutation aggravated ER stress and UPR in the partially ligated CA*

ER stress and the UPR involve the activation of three transmembrane proteins: IRE1α, protein kinase RNA-like ER kinase (PERK), and activating transcription factor 6 (ATF6). Immunoblotting results showed that after partial ligation, *Clock*$^{\Delta 19/\Delta 19}$ mutation significantly increased p-PERK and p-IRE1α protein expression of CA, whereas ATF6 showed no significant difference between *Clock*$^{\Delta 19/\Delta 19}$ and WT mice (**Figure 4A**). We also found that p-eIF2α and XBP-1, downstream targets of PERK and IRE1α respectively, were significantly upregulated in *Clock*$^{\Delta 19/\Delta 19}$ mice compared to WT mice (**Figure 4A**). Furthermore, double immunostaining

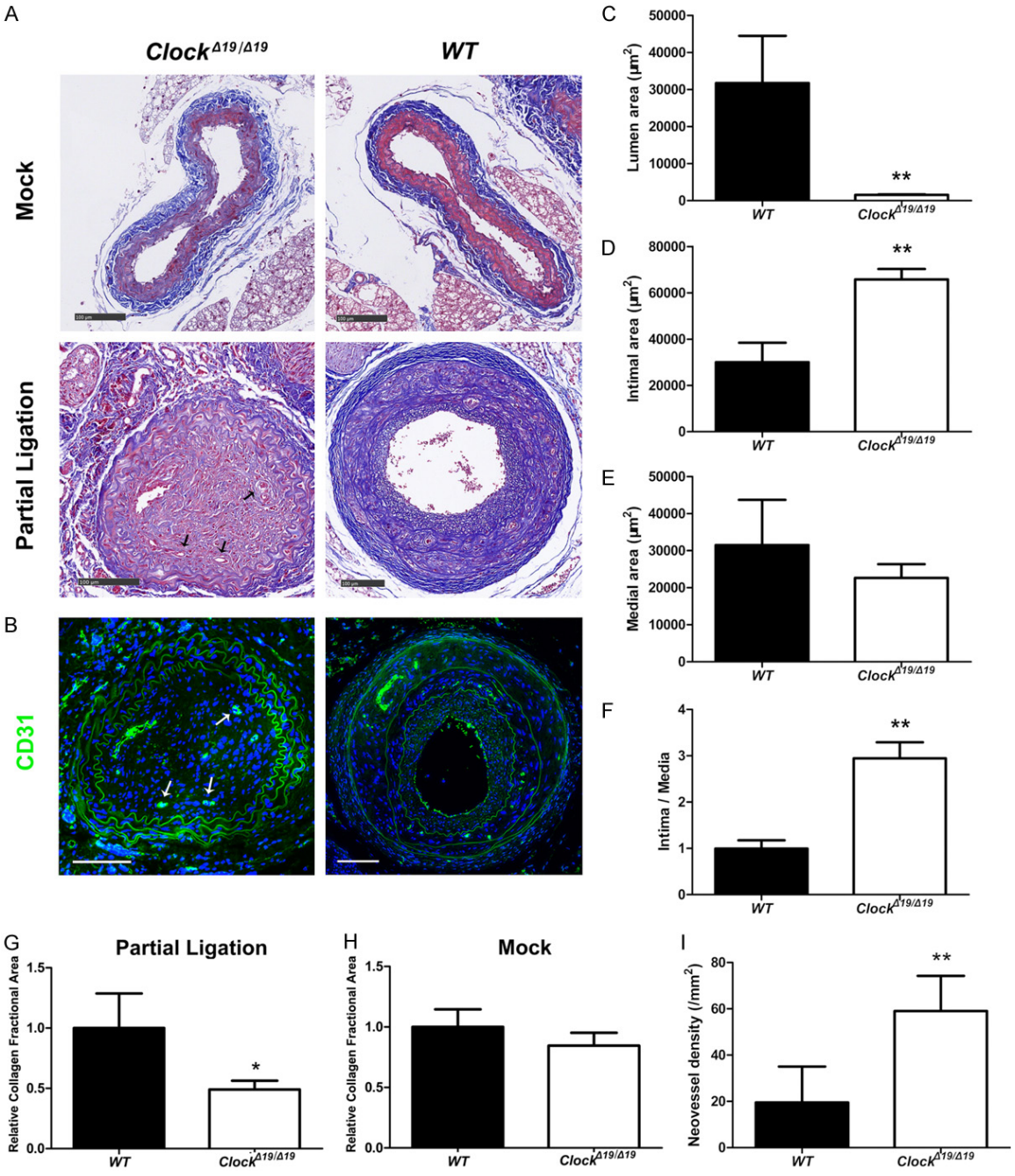

Figure 2. *Clock*$^{\Delta 19/\Delta 19}$ increased the extent of stenosis and changed the structure of the partially ligated carotid artery (CA) ligation model. A. Masson trichrome staining of mouse CA. Arrows indicate neovessels. B. Immunofluorescence staining for CD31 (green). Nuclei were stained with DAPI (blue). Arrows indicate neovessels. C-F. Mean lumen, intimal, and medial areas, and intima/media ratio (n = 6). G, H. Relative collagen fractional area of right common CAs (mock surgery, n = 6) and left common CAs (partial ligation, n = 6). I. Neovessel density of partially ligated CAs (n = 6). Scale bar: 100 mm. **P* < 0.05, ***P* < 0.01.

demonstrated that the proportion of XBP-1 (+) ECs was significantly higher in the intima of partially ligated CAs of *Clock*$^{\Delta 19/\Delta 19}$ mice than in those of WT mice (**Figure 4B**, **4C**). XBP-1 expression was also significantly increased in the intima of partially ligated CAs of *Clock*$^{\Delta 19/\Delta 19}$ mice compared to that in WT mice (**Figure 4B**, **4D**).

In vitro

Clock$^{\Delta 19/\Delta 19}$ *mutation aggravated DF-induced EndMT and ER stress:* qRT-PCR results revealed that *Clock*$^{\Delta 19/\Delta 19}$ mutation significantly aggravated DF-induced increase in expression levels of the mesenchymal markers *S100a4*, *Acta2*,

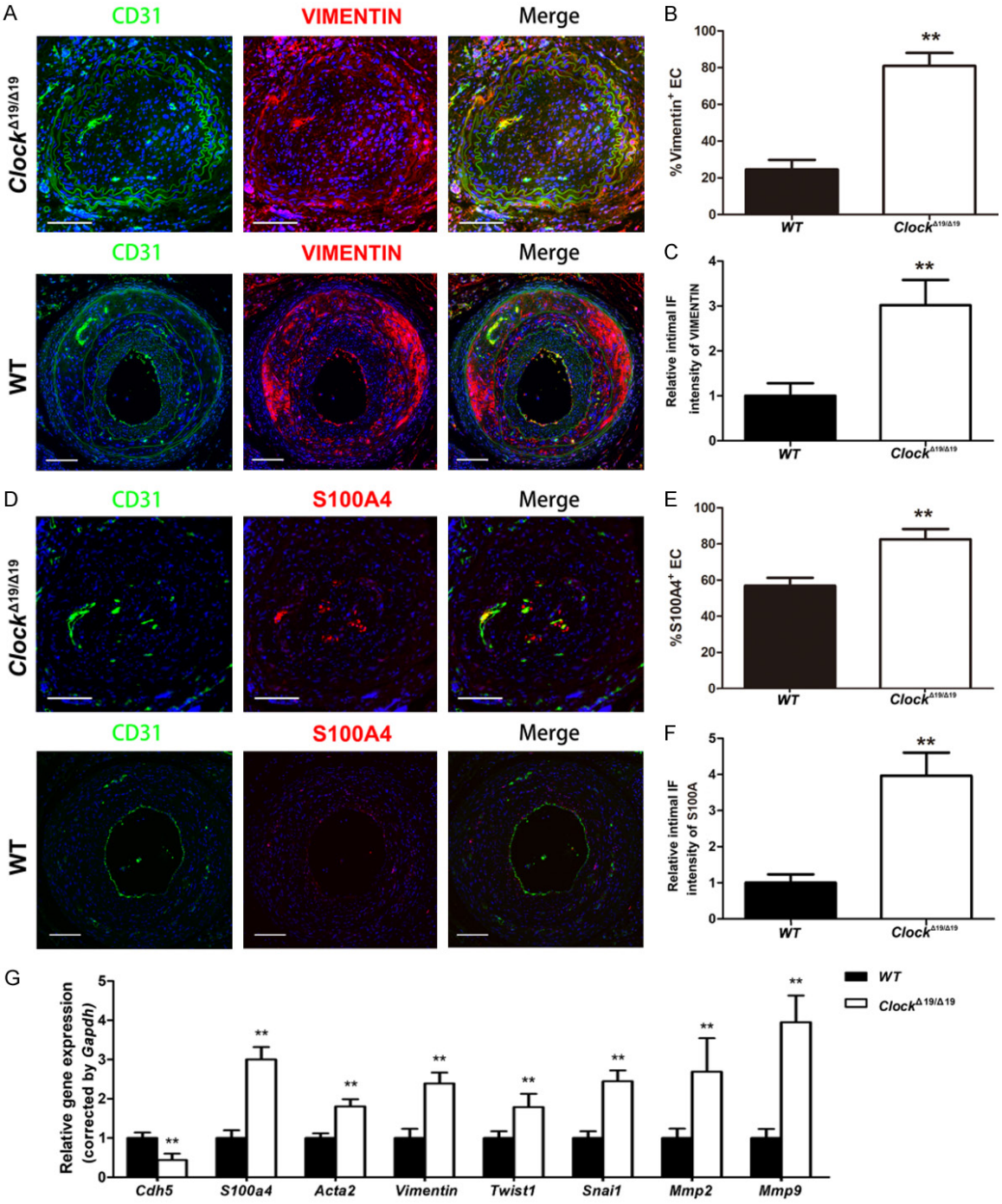

Figure 3. *Clock*$^{\Delta 19/\Delta 19}$ stimulated EndMT *in vivo*. A. Immunofluorescence staining for CD31 (green) and vimentin (red). Nuclei were stained with DAPI (blue). B. Immunocytochemical analysis of the percentages of vimentin$^+$ ECs in the intima of partially ligated CAs (n = 6). C. Immunofluorescence intensity of vimentin in the intima of partially ligated CAs (n = 6). D. Immunofluorescence staining for CD31 (green) and S100A4 (red). Nuclei were stained with DAPI (blue). E. Immunocytochemical analysis of the percentage of S100A4$^+$ ECs in the intima of partially ligated CAs (n = 6). F. Immunofluorescence intensity of S100A4 in the intima of partially ligated CAs (n = 6). G. Relative mRNA levels of *Cdh5*, *S100a4*, *Acta2*, *Vimentin*, *Twist1*, *Snai1*, *Mmp2*, and *Mmp9* in partially ligated CAs (n = 6). Scale bar: 100 μm (n = 6). **P* < 0.05, ***P* < 0.01.

vimentin, *Snai1*, *Mmp2*, and *Mmp9* and the decrease in expression levels of the endothelial marker *Cdh5* in the pMAECs (**Figure 5A**).

We also investigated the effects of CLOCK on ER stress. Western blot analyses revealed that DF significantly upregulated p-PERK, p-IRE1α,

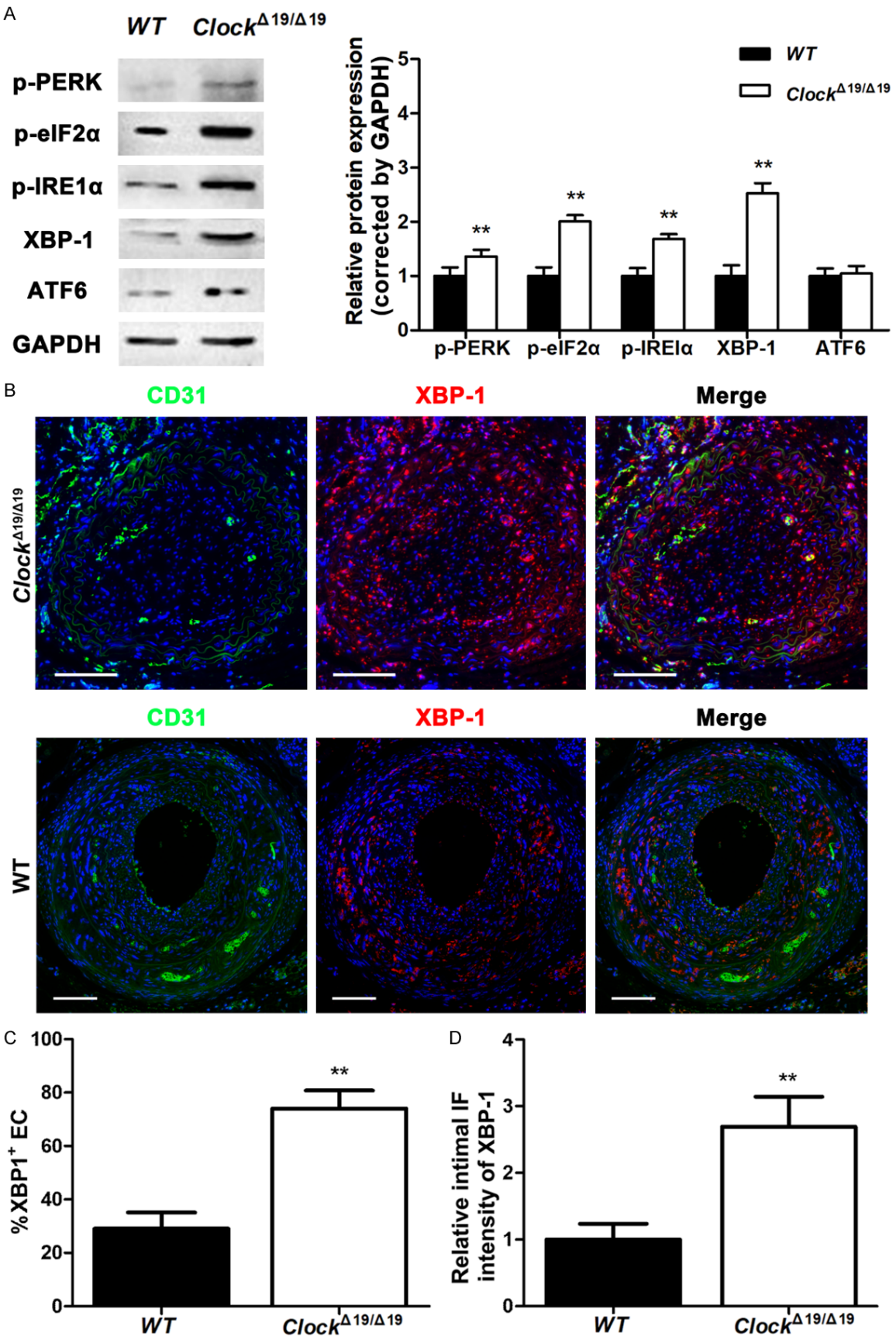
A
WT
Clock Δ19/Δ19
p-PERK
p-eIF2α
p-IRE1α
XBP-1
ATF6
GAPDH
Relative protein expression (corrected by GAPDH)
WT
Clock Δ19/Δ19
p-PERK
p-eIF2α
p-IREIα
XBP-1
ATF6
B
CD31
XBP-1
Merge
Clock Δ19/Δ19
WT
C
%XBP1+ EC
D
Relative intimal IF intensity of XBP-1

Figure 4. The *Clock*$^{\Delta 19/\Delta 19}$ mutation exacerbated endoplasmic reticulum (ER) stress and the unfolded protein response (UPR) *in vivo*. A. p-PERK, p-eIF2α, p-IRE1α, XBP-1, and ATF6 protein levels in partially ligated CAs assayed by western blotting (n = 6). B. Immunofluorescence staining for CD31 (green) and XBP-1 (red). Nuclei were stained with DAPI (blue). Scale bar: 100 μm. C. Immunocytochemical analysis of the percentage of XBP-1^{+} ECs in the intima of partially ligated CAs (n = 6). D. Immunofluorescence intensity of XBP-1 in the intima of partially ligated CAs (n = 6). *P < 0.05, **P < 0.01.

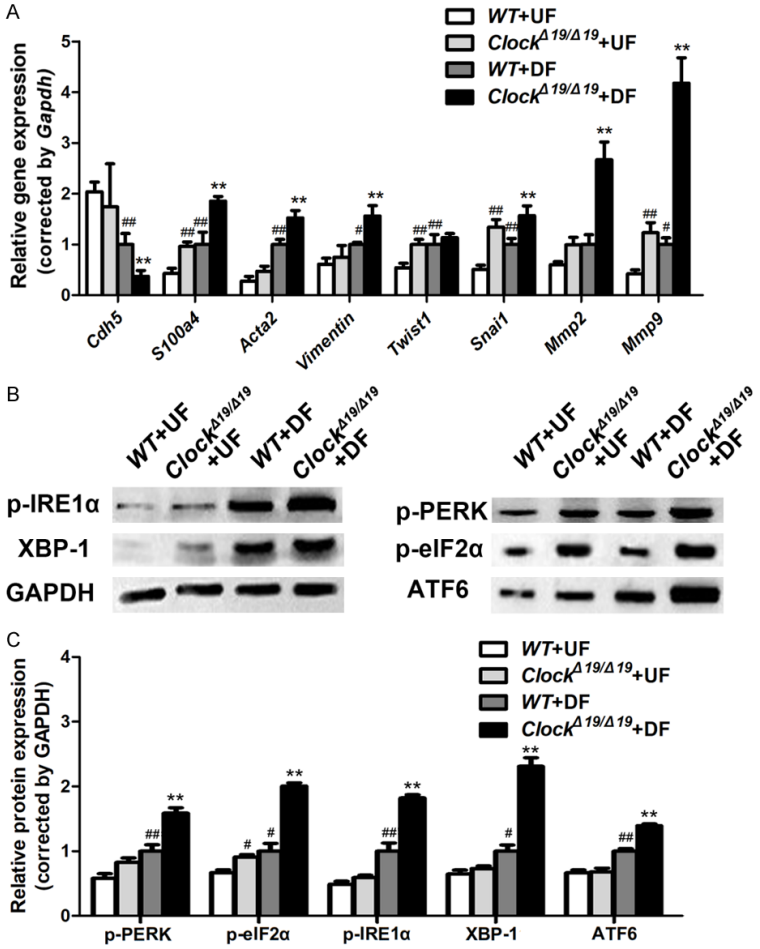

Figure 5. *Clock*$^{\Delta 19/\Delta 19}$ aggravated EndMT and endoplasmic reticulum (ER) stress induced by disturbed flow (DF) *in vitro*. A. Relative mRNA levels of *Cdh5*, *S100a4*, *Acta2*, *Vimentin*, *Twist1*, *Snai1*, *Mmp2*, and *Mmp9* in pMAECs exposed to disturbed flow (DF) or undisturbed flow (UF) (n = 3). B, C. p-PERK, p-eIF2α, p-IRE1α, XBP-1, and ATF6 protein levels of pMAECs exposed to disturbed flow (DF) or undisturbed flow (UF) assayed by western blotting (n = 3). *P < 0.05 vs. *WT*+DF, **P < 0.01 vs. *WT*+DF, $^{\#}$P < 0.05 vs. *WT*+UF, $^{\#\#}$P < 0.01 vs. *WT*+UF.

ATF6, p-eIF2α, and XBP-1 expression in the pMACEs, and *Clock*$^{\Delta 19/\Delta 19}$ mutation significantly aggravated these changes (**Figure 5B**, **5C**).

Clock$^{\Delta 19/\Delta 19}$ *mutation induced EndMT by activating the IRE1α-XBP1 axis:* To further investigate the effects of the *Clock*$^{\Delta 19/\Delta 19}$ mutation on EndMT, pMAECs exposed to DF were treated with an IRE-1α inhibitor (STF-083010; 15 or 30 μM) and PERK inhibitor (GSK-2606414; 0.015 or 0.03 μM). qRT-PCR revealed that STF-083010 significantly attenuated the decreased expression level of *Cdh5* (**Figure 6A**) and the increased expression of *S100a4, vimentin*, and *Snai1* in *Clock*$^{\Delta 19/\Delta 19}$ pMAECs exposed to DF in a dose-dependent manner (**Figure 6B-D**). However, GSK2606414 failed to rescue the aggravated EndMT in *Clock*$^{\Delta 19/\Delta 19}$ pMAECs exposed to DF despite the increased expression level of *vimentin* (**Figure 6A-D**).

Discussion

Substantial evidence over the past 20 years suggests that both circadian rhythms and ER stress participate in atherosclerosis [6, 15]. However, the molecular connections between these two signaling pathways in carotid artery stenosis remain unknown. Here, we confirmed the suppressive effects of CLOCK on carotid artery stenosis by controlling endoplasmic reticulum stress-induced endothelial-mesenchymal transition through the IRE1α-XBP1 axis.

CLOCK is a core circadian protein that regulates biological rhythms [9]. Disturbance of the CLOCK-dependent biological rhythm might be directly involved in the deterioration of physiological function and aging-related diseases [9, 16]. In this study, we found that carotid plaque LRNCs of low CLOCK level were more closely associated with LRNC size, and IPH and AHA type VI plaque, which might predict poor prognosis for patients with ICAS. To determine whether the

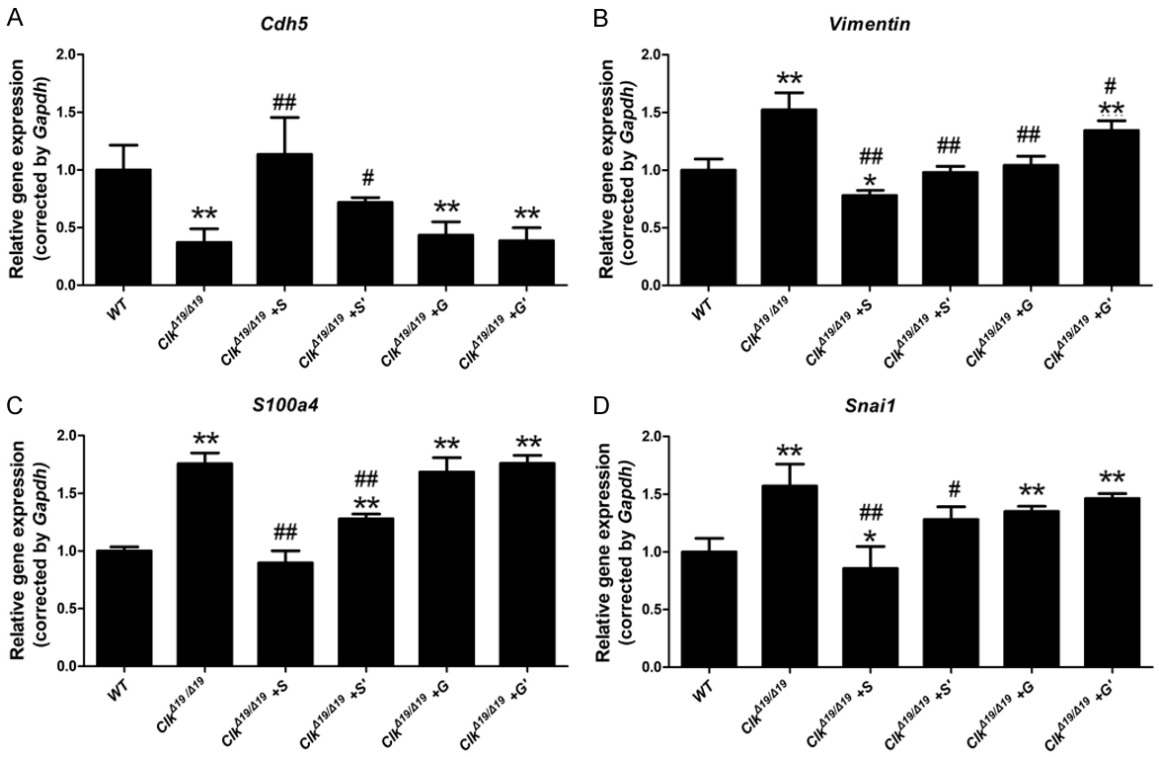

Figure 6. *Clock*$^{\Delta 19/\Delta 19}$ (*Clk*) mutation aggravated disturbed flow (DF)-induced EndMT by activating the IRE1α-XBP1 axis. Wild-type (WT) or *Clock* $^{\Delta 19/\Delta 19}$ pMAECs were exposed to disturbed flow (DF) and DMSO (WT or *Clk*), 30 μM STF-083010 (*Clk*+S), 15 μM STF-083010 (*Clk*+S'), 0.03 μM GSK2606414 (*Clk*+G), or 0.015 μM GSK2606414 (*Clk*+G') for 72 h. A-D. *Cdh5*, *S100a4*, *Vimentin*, and *Snai1* mRNA levels were assayed by quantitative reverse transcription PCR (n = 3). **P* < 0.05 vs. *WT*, ***P* < 0.01 vs. *WT*, $^{\#}P$ < 0.05 vs. *Clk*, $^{\#\#}P$ < 0.01 vs. *Clk*.

mutational disruption of *CLOCK* can lead to carotid artery stenosis, *Clock*$^{\Delta 19/\Delta 19}$ mice were employed to establish a partial ligation model to mimic the disrupted blood flow of carotid artery stenosis [12]. Consistent with the results of previous studies [17, 18], our *in vivo* results showed that *Clock*$^{\Delta 19/\Delta 19}$ mice had significantly increased neointima formation compared to WT mice in the partially ligated CAs, and the *Clock*$^{\Delta 19/\Delta 19}$ mutation led to decreased collagen content and increased neovascularization in partially ligated CAs. Thus, CLOCK may play an important role in suppressing carotid artery stenosis and plaque vulnerability.

We next sought to determine the mechanism by which CLOCK suppresses carotid artery stenosis. Using chronological *in vivo* imaging, a recent study showed that endothelial inflammation occurs earlier than neutrophil accumulation and lipid deposition in zebrafish fed a high-fat, cholesterol-rich diet [19], emphasizing the important role of the vascular endothelium in cardiovascular homeostasis. Several studies indicate that the EndMT of ECs plays a key role in atherosclerosis progression [20, 21]. EndMT is an extreme form of endothelial cell plasticity [22], which can be promoted by hypoxia, high glucose, and disrupted blood flow [23]. Here, the *Clock*$^{\Delta 19/\Delta 19}$ mutation resulted in increased EndMT *in vitro* and *in vivo*. EndMT is widely known to be associated with angiogenesis and an altered balance of collagen-matrix metalloproteinases [21, 24, 25], which might explain the decreased collagen content and increased neovascularization observed in partially ligated CAs from *Clock*$^{\Delta 19/\Delta 19}$ mice.

Hydrodynamic shear stress regulates inflammation in human aortic ECs through ER stress by activating transcription factor x-box binding protein 1 (XBP1) [3], and the regulatory role of *CLOCK* in ER stress has been demonstrated [4, 26]. Thus, *CLOCK* might be involved in carotid artery stenosis via the regulation of ER stress, as evidenced in the present study. We evaluated the effect of *Clock*$^{\Delta 19/\Delta 19}$ on ER stress *in vivo* and *in vitro* and found that *Clock*$^{\Delta 19/\Delta 19}$ resulted

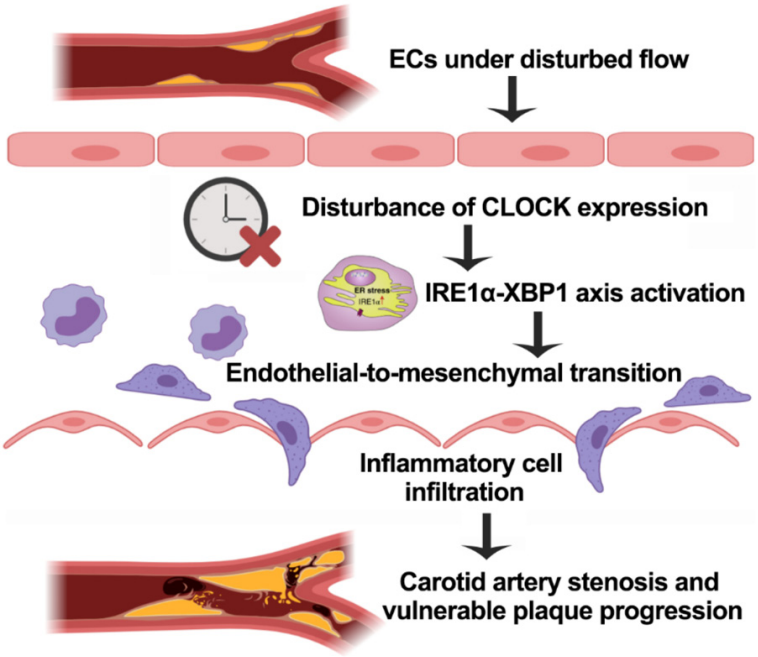

Figure 7. The mechanism for the inhibitory effect of CLOCK as a suppressor of carotid plaque progression. Under disturbed flow, the disturbance of endothelial CLOCK expression activates the IRE1α-XBP1 axis and then leads to endothelial-to-mesenchymal transition; this results in increased inflammation. The results of our research showed that CLOCK attenuated carotid plaque stenosis and vulnerable plaque progression through the signaling pathways above.

in the activation of the IRE1α-XBP1 and PERK-eIF2α signaling pathways *in vivo* and *in vitro*. The activation of these pathways is known to induce apoptosis and angiogenesis [27, 28]. Our results showing increased LRNC size and IPH in human plaques and increased neovascularization in partial ligated CAs of *Clock*$^{\Delta 19/\Delta 19}$ mice are consistent with this mechanism. Moreover, ER stress has been found to induce the expression of the EndMT transcription factor SNAI1 [29]. SNAI1 activation by ER stress promotes arterial endothelial EndMT of plaques. The present study also showed the regulatory effect of the IRE1α-XBP1 axis on EndMT by investigating the rescue effect of the IRE-1α inhibitor and the PERK inhibitor on DF-induced EndMT in *Clock*$^{\Delta 19/\Delta 19}$ pMAECs. Only the IRE-1α inhibitor successfully and significantly attenuated the EndMT caused by *Clock*$^{\Delta 19/\Delta 19}$ mutation, which might be due to the regulatory effects of the IRE1α-XBP1 axis on endothelial apoptosis and migration [30, 31]. It is also interesting to note that *Clock*$^{\Delta 19/\Delta 19}$ increased ATF6 expression in pMAECs but failed to increase ATF6 expression in the partially ligated CAs of the mice. The difference between our *in vivo* and *in vitro* results might be attributed to the suppression of ATF6 by a cholesterol-enriched diet and/or the influence of other (non-EC) components within the artery [32].

This study has a few limitations. First, the mouse CA partial ligation model might differ from a traditional mouse model of atherosclerosis induced by a high-fat diet only. However, this CA partial ligation model has been proved effective in studies on the mechanism of atherosclerotic plaque progression [12, 33, 34]. Second, the molecular mechanisms between CLOCK and the IRE1α-XBP1 axis are complex, warranting additional studies to elucidate the relevant mechanisms.

Nevertheless, loss of *CLOCK* function activated the IRE1α-XBP1 axis and subsequently increased SNAI1 expression, thereby stimulating the EndMT of ECs under DF. These findings suggest that CLOCK functions as a suppressor of carotid artery stenosis (**Figure 7**). Further analysis of the molecular mechanisms focusing on the CLOCK-IRE1α-XBP1 axis is needed to develop promising therapies for carotid artery stenosis.

Acknowledgements

We thank Drs. Yong Ding and Yifan Liu for their assistance in human sample curation and Dr. Mengjiao Zhu for the technical advice on immunofluorescence and confocal microscopy analyses. This work was supported by grants from Shanghai Sailing Program (Grant No. 20YF1406700), the National Natural Science Foundation of China (Grant No. 81970408), and Science and Technology Commission of Shanghai Municipality (Grant No. 19411966900).

Disclosure of conflict of interest

None.

Address correspondence to: Drs. Daqiao Guo and Xiao Tang, Department of Vascular Surgery, Institute of Vascular Surgery, Zhongshan Hospital, Fudan University, 180 Fenglin Road, Shanghai 200032, China. Tel: +86-13801785258; Fax: +86-021-64041990-2819; E-mail: guo.daqiao@zs-hospital.sh.cn (DQG); Tel: +86-13918416387; Fax: +86-021-64041990-2819; E-mail: tang.xiao@zs-hospital.sh.cn (XT); Dr. Pengfei Zhang, Department of Thoracic and Cardiovascular Surgery, The Affiliated Drum Tower Hospital, Medical School of Nanjing University, 321 Zhongshan Road, Nanjing 210008, China. Tel: +86-15996291285; Fax: +86-025-68182222; E-mail: zhangpfnju@gmail.com

References

[1] Zhou C, Yuan C, Li R, Wang W, Li C and Zhao X; CARE-II Study Collaborators. Association between incomplete circle of Willis and carotid vulnerable atherosclerotic plaques. Arterioscler Thromb Vasc Biol 2018; 38: 2744-2749.

[2] Tang H, Zhu M, Zhao G, Fu W, Shi Z, Ding Y and Guo D. Loss of CLOCK under high glucose upregulates ROCK1-mediated endothelial to mesenchymal transition and aggravates plaque vulnerability. Atherosclerosis 2018; 275: 58-67.

[3] Bailey KA, Moreno E, Haj FG, Simon SI and Passerini AG. Mechanoregulation of p38 activity enhances endoplasmic reticulum stress-mediated inflammation by arterial endothelium. FASEB J 2019; 33: 12888-12899.

[4] Battson ML, Lee DM and Gentile CL. Endoplasmic reticulum stress and the development of endothelial dysfunction. Am J Physiol Heart Circ Physiol 2017; 312: H355-H367.

[5] Hutt DM, Powers ET and Balch WE. The proteostasis boundary in misfolding diseases of membrane traffic. FEBS Lett 2009; 583: 2639-2646.

[6] Hotamisligil GS. Endoplasmic reticulum stress and atherosclerosis. Nat Med 2010; 16: 396-399.

[7] Moore PC and Oakes SA. CPEB4 links the clock and the UPR to protect the liver. Nat Cell Biol 2017; 19: 79-81.

[8] Bell-Pedersen D, Cassone VM, Earnest DJ, Golden SS, Hardin PE, Thomas TL and Zoran MJ. Circadian rhythms from multiple oscillators: lessons from diverse organisms. Nat Rev Genet 2005; 6: 544-556.

[9] Zhao J, Warman GR and Cheeseman JF. The functional changes of the circadian system organization in aging. Ageing Res Rev 2019; 52: 64-71.

[10] Naylor AR, Ricco JB, de Borst GJ, Debus S, de Haro J, Halliday A, Hamilton G, Kakisis J, Kakkos S, Lepidi S, Markus HS, McCabe DJ, Roy J, Sillesen H, van den Berg JC, Vermassen F; Esvs Guidelines Committee, Kolh P, Chakfe N, Hinchliffe RJ, Koncar I, Lindholt JS, Vega de Ceniga M, Verzini F; Esvs Guideline Reviewers, Archie J, Bellmunt S, Chaudhuri A, Koelemay M, Lindahl AK, Padberg F and Venermo M. Editor's choice - management of atherosclerotic carotid and vertebral artery disease: 2017 clinical practice guidelines of the European society for vascular surgery (ESVS). Eur J Vasc Endovasc Surg 2018; 55: 3-81.

[11] King DP, Zhao Y, Sangoram AM, Wilsbacher LD, Tanaka M, Antoch MP, Steeves TD, Vitaterna MH, Kornhauser JM, Lowrey PL, Turek FW and Takahashi JS. Positional cloning of the mouse circadian clock gene. Cell 1997; 89: 641-653.

[12] Nam D, Ni CW, Rezvan A, Suo J, Budzyn K, Llanos A, Harrison D, Giddens D and Jo H. Partial carotid ligation is a model of acutely induced disturbed flow, leading to rapid endothelial dysfunction and atherosclerosis. J Physiol Heart Circ Physiol 2009; 297: H1535-H1543.

[13] He D, Zhao M, Wu C, Zhang W, Niu C, Yu B, Jin J, Ji L, Willard B, Mathew AV, Chen YE, Pennathur S, Yin H, He Y, Pan B and Zheng L. Apolipoprotein A-1 mimetic peptide 4F promotes endothelial repairing and compromises reendothelialization impaired by oxidized HDL through SR-B1. Redox Biol 2018; 15: 228-242.

[14] Warboys CM, de Luca A, Amini N, Luong L, Duckles H, Hsiao S, White A, Biswas S, Khamis R, Chong CK, Cheung WM, Sherwin SJ, Bennett MR, Gil J, Mason JC, Haskard DO and Evans PC. Disturbed flow promotes endothelial senescence via a p53-dependent pathway. Arterioscler Thromb Vasc Biol 2014; 34: 985-995.

[15] Yang G, Zhang J, Jiang T, Monslow J, Tang SY, Todd L, Puré E, Chen L and FitzGerald GA. Bmal1 deletion in myeloid cells attenuates atherosclerotic lesion development and restrains abdominal aortic aneurysm formation in hyperlipidemic mice. Arterioscler Thromb Vasc Biol 2020; 40: 1523-1532.

[16] Anea CB, Zhang M, Stepp DW, Simkins GB, Reed G, Fulton DJ and Rudic RD. Vascular disease in mice with a dysfunctional circadian clock. Circulation 2009; 119: 1510-1517.

[17] Jiang Q, Liu H, Wang S, Wang J, Tang Y, He Z, Wu F, Huang Z, Cong X, Ding R and Liang C. Circadian locomotor output cycles kaput accelerates atherosclerotic plaque formation by upregulating plasminogen activator inhibitor-1 expression. Acta Biochim Biophys Sin (Shanghai) 2018; 50: 869-879.

[18] Pan X, Jiang XC and Hussain MM. Impaired cholesterol metabolism and enhanced athero-

sclerosis in clock mutant mice. Circulation 2013; 128: 1758-1769.
[19] Luo H, Li QQ, Wu N, Shen YG, Liao WT, Yang Y, Dong E, Zhang GM, Liu BR, Yue XZ, Tang XQ and Yang HS. Chronological in vivo imaging reveals endothelial inflammation prior to neutrophils accumulation and lipid deposition in HCD-fed zebrafish. Atherosclerosis 2019; 290: 125-135.
[20] Chen PY, Qin L, Baeyens N, Li G, Afolabi T, Budatha M, Tellides G, Schwartz MA and Simons M. Endothelial-to-mesenchymal transition drives atherosclerosis progression. J Clin Invest 2015; 125: 4514-4528.
[21] Evrard SM, Lecce L, Michelis KC, Nomura-Kitabayashi A, Pandey G, Purushothaman KR, d'Escamard V, Li JR, Hadri L, Fujitani K, Moreno PR, Benard L, Rimmele P, Cohain A, Mecham B, Randolph GJ, Nabel EG, Hajjar R, Fuster V, Boehm M and Kovacic JC. Endothelial to mesenchymal transition is common in atherosclerotic lesions and is associated with plaque instability. Nat Commun 2016; 7: 11853.
[22] van Meeteren LA and ten Dijke P. Regulation of endothelial cell plasticity by TGF-β. Cell Tissue Res 2012; 347: 177-186.
[23] Moonen JR, Lee ES, Schmidt M, Maleszewska M, Koerts JA, Brouwer LA, van Kooten TG, van Luyn MJ, Zeebregts CJ, Krenning G and Harmsen MC. Endothelial-to-mesenchymal transition contributes to fibro-proliferative vascular disease and is modulated by fluid shear stress. Cardiovasc Res 2015; 108: 377-386.
[24] Sun JX, Chang TF, Li MH, Sun LJ, Yan XC, Yang ZY, Liu YS, Xu WQ, Lv Y, Su JB, Liang L, Han H, Dou GR and Wang YS. SNAI1, an endothelial-mesenchymal transition transcription factor, promotes the early phase of ocular neovascularization. Angiogenesis 2018; 21: 635-652.
[25] Tanaka M, Koyama T, Sakurai T, Kamiyoshi A, Ichikawa-Shindo Y, Kawate H, Liu T, Xian X, Imai A, Zhai L, Hirabayashi K, Owa S, Yamauchi A, Igarashi K, Taniguchi S and Shindo T. The endothelial adrenomedullin-RAMP2 system regulates vascular integrity and suppresses tumour metastasis. Cardiovasc Res 2016; 111: 398-409.
[26] Ohta Y, Taguchi A, Matsumura T, Nakabayashi H, Akiyama M, Yamamoto K and Tanizawa Y. Clock gene dysregulation induced by chronic ER stress disrupts β-cell function. EBioMedicine 2017; 18: 146-156.
[27] Liu C, Liu Y, He J, Mu R, Di Y, Shen N, Liu X, Gao X, Wang J, Chen T, Fang T, Li H and Tian F. Liraglutide increases VEGF expression via CNPY2-PERK pathway induced by hypoxia/reoxygenation injury. Front Pharmacol 2019; 10: 789.
[28] Wang X, Xia HY, Qin HY, Kang XP, Hu HY, Zheng J, Jiang JY, Yao LA, Xu YW, Zhang T and Zhang XL. 20(S)-protopanaxadiol induces apoptosis in human umbilical vein endothelial cells by activating the PERK-eIF2alpha-ATF4 signaling pathway. J Cell Biochem 2019; 120: 5085-5096.
[29] Liu J, Wu Z, Han D, Wei C, Liang Y, Jiang T, Chen L, Sha M, Cao Y, Huang F, Geng X, Yu J, Shen Y, Wang H, Feng L, Wang D, Fang S, Wang S and Shen Y. Mesencephalic astrocyte-derived neurotrophic factor inhibits liver cancer through small ubiquitin-related modifier (SUMO)ylation-related suppression of NF-κB/Snail signaling pathway and epithelial-mesenchymal transition. Hepatology 2020; 71: 1262-1278.
[30] Anspach L, Tsaryk R, Seidmann L, Unger RE, Jayasinghe C, Simiantonaki N, Kirkpatrick CJ and Pröls F. Function and mutual interaction of BiP-, PERK-, and IRE1α-dependent signaling pathways in vascular tumours. J Pathol 2020; 251: 123-134.
[31] Yang J, Xu J, Danniel M, Wang X, Wang W, Zeng L and Shen L. The interaction between XBP1 and eNOS contributes to endothelial cell migration. Exp Cell Res 2018; 363: 262-270.
[32] Tumanovska LV, Swanson RJ, Serebrovska ZO, Portnichenko GV, Goncharov SV, Kysilov BA, Moibenko OO and Dosenko VE. Cholesterol enriched diet suppresses ATF6 and PERK and upregulates the IRE1 pathways of the unfolded protein response in spontaneously hypertensive rats: relevance to pathophysiology of atherosclerosis in the setting of hypertension. Pathophysiology 2019; 26: 219-226.
[33] Schürmann C, Dienst FL, Pálfi K, Vasconez AE, Oo JA, Wang S, Buchmann GK, Offermanns S, van de Sluis B, Leisegang MS, Günther S, Humbert PO, Lee E, Zhu J, Weigert A, Mathoor P, Wittig I, Kruse C and Brandes RP. The polarity protein Scrib limits atherosclerosis development in mice. Cardiovasc Res 2019; 115: 1963-1974.
[34] Seo Y, Park J, Choi W, Ju Son D, Sung Kim Y, Kim MK, Yoon BE, Pyee J, Tae Hong J, Go YM and Park H. Antiatherogenic effect of resveratrol attributed to decreased expression of ICAM-1 (intercellular adhesion molecule-1). Arterioscler Thromb Vasc Biol 2019; 39: 675-684.